



# Transflective spin-orbital angular momentum conversion device by three-dimensional multilayer liquid crystalline materials

TIEGANG LIN,<sup>1</sup> YAQIN ZHOU,<sup>1</sup> YIDE YUAN,<sup>1</sup> WENXING FU,<sup>1</sup> LISHUANG YAO,<sup>2,3</sup> HUIHUI HUANG,<sup>1</sup> FAN FAN,<sup>1,\*</sup> AND SHUANGCHUN WEN<sup>1</sup>

<sup>1</sup>Key Laboratory for Micro-/Nano- Optoelectronic Devices of Ministry of Education, School of Physics and Electronics, Hunan University, Changsha 410082, China

<sup>2</sup>State Key Laboratory of Applied Optics, Changchun Institute of Optics, Fine Mechanics and Physics, Chinese Academy of Science, Changchun 130033, China

<sup>3</sup>yaols@ciomp.ac.cn

\*ffan@hnu.edu.cn

**Abstract:** In this paper, a liquid crystal device for generating transflected optical vortices with high efficiency based on Pancharatnam-Berry phase is devised and demonstrated experimentally. In the experiment, both photo-alignment material and polymer-alignment material are used for assembling three-dimensional distributed liquid crystal polymer and cholesteric liquid crystal. Through the interaction between the incident light and the device, both transmitted light and reflected light get spin-orbital angular momentum conversion. Moreover, the amount of transmitted and reflected beams can be modulated by the input polarization. In our proposal, the device is dual functional, low-cost and simple in manufacturing process.

© 2018 Optical Society of America under the terms of the [OSA Open Access Publishing Agreement](#)

## 1. Introduction

Each left-handed circularly (LHC) or right-handed circularly (RHC) polarized photon carrying a quantized spin angular momentum of  $+$  or  $-\hbar$  respectively, corresponds to a mutually orthogonal state of polarization [1]. Vortex beam is a beam with a characteristic helical wavefront, whose phase changes by  $\pm 2\pi m$  for integer  $m$  around the phase singularity at the beam axis. The electric field of a vortex beam depends on the azimuth angle  $\varphi$  and can be written as  $E(r, \varphi) = E_0(r, \varphi) \exp(im\varphi)$ . It has been shown that each photon in the  $m$ th mode carries an orbital angular momentum of  $m\hbar$  [2,3]. The light beam with helical wavefront exhibits a dark spot in the center, and a ring-like intensity profile [3,4].

Liquid crystal (LC) q-plate is well-known owing to its ability of generating a vortex beam of  $m = \pm 2q$  that the sign depends on the handedness of the circular polarization of the incident beam, where  $q$  is an integer or half-integer to avoid discontinuous line in the plane. It is defined as a birefringent LC plate having an azimuthal distribution of the local optical axis in the transverse plane. Meanwhile, it carries a topological singularity of charge  $q$  at its center, that is, the LC molecular orientation angle can be expressed by the equation:  $\theta(r, \varphi) = q\varphi + \theta_0$ , where  $\theta_0$  is a constant [4].

For nematic liquid crystal (NLC) q-plate with half wave birefringent phase retardation, an incident circularly polarized light emerges from it with the orthogonal state and an additional geometrical phases. Here, NLC q-plate operates at a specific wavelength, and requires precise fabrication for the full spin-orbital angular momentum conversion efficiency [5,6]. Moreover, two opposite orbital states generated by linearly polarized light interacting with the q-plate can't be separated spatially without additional devices. Planar texture cholesteric liquid crystal (ChLC), as a stratified and anisotropic media, has the selectivity of circular polarized

light in the Bragg regime when the wavelength  $\lambda$  satisfies the condition:  $n_o p < \lambda < n_e p$ , where  $p$  is the pitch of ChLC, besides,  $n_e$  and  $n_o$  are extraordinary and ordinary refractive indices of liquid crystal materials. Bragg reflection occurs for normally incident light with the same circular polarization handedness as the helix, further, new findings were put forward recently that the reflected optical phase is twice the value of helix phase [7,8]. The fabrication of ChLC q-plate and the study of reflective spin-orbital angular momentum conversion from ChLC medium were recorded [9–13]. In general, since the conversion efficiency depends on the reflectivity of the ChLC, the theoretically conversion efficiency ideally tends asymptotically to 100% as the thickness increases. In contrast to NLC q-plate, ChLC vortex generator gives rise to a polarization controlled transformation of orbital angular momentum via polarization-preserving (Bragg) reflection of input circularly polarized light. Moreover, the reflection scheme of vortex generation is no longer subject to strict condition on the birefringent layer thickness. However, the spin-orbital angular momentum conversion efficiency of ChLC is limited because the transmissive phase is insensitive to the helix phase. Recently, a solution to improve the efficiency for any circularly polarized light was designed by using a cholesteric slab sandwiched between a substrate and a rear mirror [14], nevertheless, the two opposite orbital states are still spatially inseparable when linearly polarized light illuminates the slab.

Many potential applications based on vortex beams were found in tweezers, microscopy, optical manipulation, communication and quantum information processing [15–18]. Hence, generation and manipulation of optical vortices have attracted much attention. Subsequently, many vortex-relevant optical integrated elements such as bifocal vortex lens [19], fork grating [20], and forked vortex lens [21] were proposed in recent years to improve the efficiency of spin-orbital angular momentum conversion or spatially separate the two opposite orbital states, nevertheless, their optical vortices were deflected, focused or defocused. In many occasions, multifunctional integrated LC devices can be fabricated via using the technology of photo-alignment or stacking multilayer polymer thin film [19–23].

In our work, we present an integrated LC optical device, which splits two orthogonal circularly polarized light forward and backward, moreover, spin angular momentum carried by circularly polarized light is converted into orbital angular momentum through the interaction of light with device, and the transmissive and reflective orbital angular momenta have the same change amount. Optical vortices are generated and manipulated by means of controlling the rotate state of LC molecules in the direction which is perpendicular to the cell. In this manner, planar-type wavefronts are changed into the spiral modes on the two sides after interacting with this integrated transfective q-plate. In our experiment, it was firstly proposed that the element with specific structure can be fabricated by integrating LC polymer and ChLC together. The experiment proved that the transfective q-plate is high-efficient, low-cost and easy in fabrication.

## 2. Theory

Now we calculate the optical propagation based on polarization states in the established reference frame  $(x, y, z)$ . A circular polarization state with helicity  $\sigma = \pm 1$  can be read as:  $\vec{e}_\sigma = (\vec{x} + i\sigma\vec{y})/\sqrt{2}$ . Here, we define the handedness of circular polarization by using the sense of revolution of the electric field vector in light's propagation direction [12]. It can be formulated into  $a\vec{e}_{\sigma=1} + b\vec{e}_{\sigma=-1}$  for an arbitrary polarization state on the Poincare sphere, where  $a$  and  $b$  are complex quantities. The relationship between them can be formulated into the mathematical expression:  $|a|^2 + |b|^2 = 1$ . Thus, the planar incident wave for arbitrary polarization propagated along the positive direction of  $z$ -axis can be expressed as  $\vec{E}_{in} = E_0(a\vec{e}_{\sigma=1} + b\vec{e}_{\sigma=-1})e^{i(kz - \omega t)}$ , where  $E_0$  is an electric field amplitude.

The molecular array of transfective pancharatnam-Berry phase element is designed via integrating the conventional reflective Pancharatnam-Berry (PB) phase element and transmissive PB phase element together. Hence, we consider the optical propagation in ChLC firstly. As shown in Fig. 1(a), the optical axis of LC molecules at its front face is orientated at an angle  $\theta$  with the x-axis, makes the right-handed helix in space, and its thickness  $d_1 > 10p$  to maximize the Bragg reflection for light that having the helicity  $\sigma = -1$ . On the one hand, circularly polarized incident light with helicity  $\sigma = -1$  is reflected from ChLC device and preserves its helicity. The orientation angle  $\theta$  in the front face of ChLC cell leads to the production of a Berry phase  $\phi_B = 2\sigma\theta$  for the reflected light. On the other hand, circularly polarized light with helicity  $\sigma = 1$  passes through the ChLC device and the transmissive light preserves the helicity and cannot lead to the Berry phase. It indicates that the reflected light has the ability to obtain orbital angular momentum by light with planar wavefront interacting with Bragg-Berry reflective q-plate.

Then, we consider the condition that the optical transmission in NLC waveplate as shown in Fig. 1(b). The optical axis of LC molecules at its front face is orientated at an angle  $\theta$  with the x-axis and the thickness of NLC satisfies half waveplate retardation condition:  $2\pi(n_e^{NLC} - n_o^{NLC})d_2 / \lambda_0 = \pi$ , where  $\lambda_0$  is the wavelength of incident light. Optical transmission details of half waveplate can be calculated by rotate Jones matrix and the transmission matrix  $T$  can be expressed as:

$$T = \begin{bmatrix} \cos\theta & -\sin\theta \\ \sin\theta & \cos\theta \end{bmatrix} \begin{bmatrix} 1 & 0 \\ 0 & \exp(i\pi) \end{bmatrix} \begin{bmatrix} \cos\theta & \sin\theta \\ -\sin\theta & \cos\theta \end{bmatrix}. \quad (1)$$

As for the electric field of an incident circularly polarized beam with helicity  $\sigma = \pm 1$ , transmissive wave can be expressed as  $\vec{E}_{out} = T\vec{E}_{in}$ . Hence, light flips its spin state from  $\sigma$  to  $-\sigma$  and produces a Berry phase  $\phi_B = 2\sigma\theta$  after passing through the NLC half waveplate. Therefore, it clearly indicates that the transmitted light can get spin to orbital angular momentum conversion. The orbital angular momentum of transmissive light has an change amount of  $m = 2\sigma q$  by circularly polarized light with planar wavefront interacting with NLC q-plate [4,24].

Lastly, optical propagation is studied in the LC media where the molecular arrays are designed via assembling NLC and ChLC q-plate scheme together. The direction angle with x-axis can be described as:

$$\theta = \begin{cases} \frac{2\pi}{p}z + q\varphi + \theta_0, & 0 < z < d_1 \\ \frac{2\pi}{p}d_1 + q\varphi + \theta_0, & d_1 < z < d_1 + d_2 \end{cases}. \quad (2)$$

Figure. 1(c) shows one of the cases that  $q = 1$ ,  $\theta_0 = 0$ . Moreover,  $d_1$  is an integer multiple of  $p/2$  so that the distribution of orientation angle  $\theta_{z=0}$  and  $\theta_{z=d_1}$  in the transverse surface are the same, that is  $\theta_s = \theta_{z=0} = \theta_{z=d_1} = q\varphi + \theta_0$ . It can be achieved via alignment technology in our experiment. The direction angle in the front of the transverse surface is shown in Fig. 1(d). Besides,  $d_1$  and  $d_2$  are equal to the thickness of ChLC and NLC half waveplate respectively and represent the helical and non-helical parts respectively. Furthermore, the light wavelength  $\lambda_0$  should be in the region of  $n_o^{ChLC}p \sim n_e^{ChLC}p$  and equal to  $2(n_e^{NLC} - n_o^{NLC})d_2$ , here, birefringence parameters of the two materials may be not the same

( $n_{e,o}^{ChLC} \neq n_{e,0}^{NLC}$ ). The device is designed for the purpose of generating transmitted light and reflected light with helical wavefronts. The optical propagation through the system depicted in Fig. 1(c) is studied on the basis of photonics of NLC and right-handed ChLC. On the one hand, RHC polarized incident light with the helicity  $\sigma = -1$  is reflected and the reflected beam is expressed as  $\vec{E}_r = E_0 b \vec{e}_{\sigma=-1} e^{-2i\theta_s} e^{i(-kz - \omega t)}$  [8]. Since the reflected light propagates along the negative direction of z-axis, the reflected light is still RHC polarized and the reflective wavefront is shaped into the helical modes with topological charge  $m = 2q = 2$ . On the other hand, LHC polarized incident light with the helicity  $\sigma = 1$  is transmitted. Based on Eq. (1), the transmissive light beam can be read as  $\vec{E}_t = E_0 a \vec{e}_{\sigma=1} e^{2i\theta_s} e^{i(kz - \omega t)}$  after light interacting with the NLC layer. The transmitted light is RHC polarized and the transmissive wavefront is shaped into the helical modes with topological charge  $m = 2q = 2$ . Therefore, it manifests that the transmissivity and reflectivity are polarization-dependent, that is, they can be manipulated by the polarization state of incident light.

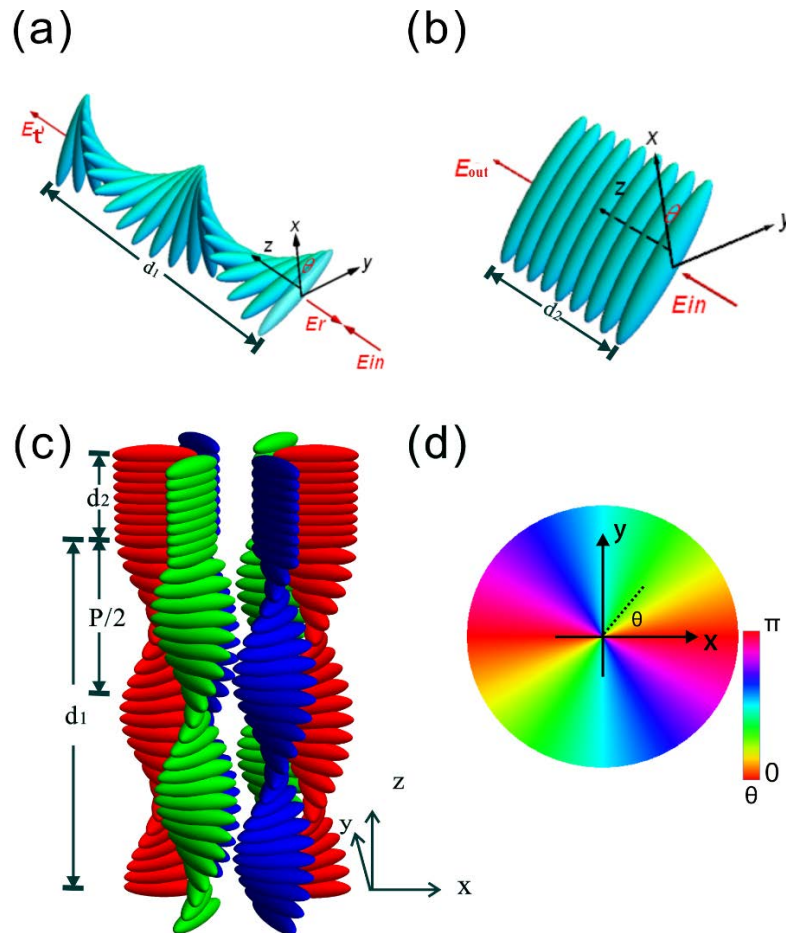


Fig. 1. (a) and (b) schematic representation of ChLC and NLC molecular orientation and light interaction with them. Schematic representation of molecular orientation in the bulk (c) and at the boundaries (d) of transfective q-plate of  $q = 1$  and  $\theta_0 = 0$ .

Based on the calculation above, the behavior of light interacting with the device is illustrated in Fig. 2. The blue and pink rectangles represent ChLC and NLC layers

respectively. Green and yellow rectangles represent the glass substrates and photo-alignment layers. It can be seen that the incident light interacts with the ChLC and then the NLC. The transfective q-plate can split two orthogonal circular polarization states on two sides, and the handedness of the transfectured beams are converted into circularly polarized handedness the same as the chiral helix of ChLC. Moreover, the transmitted vortex beam and reflected vortex beam have the same topological charges.

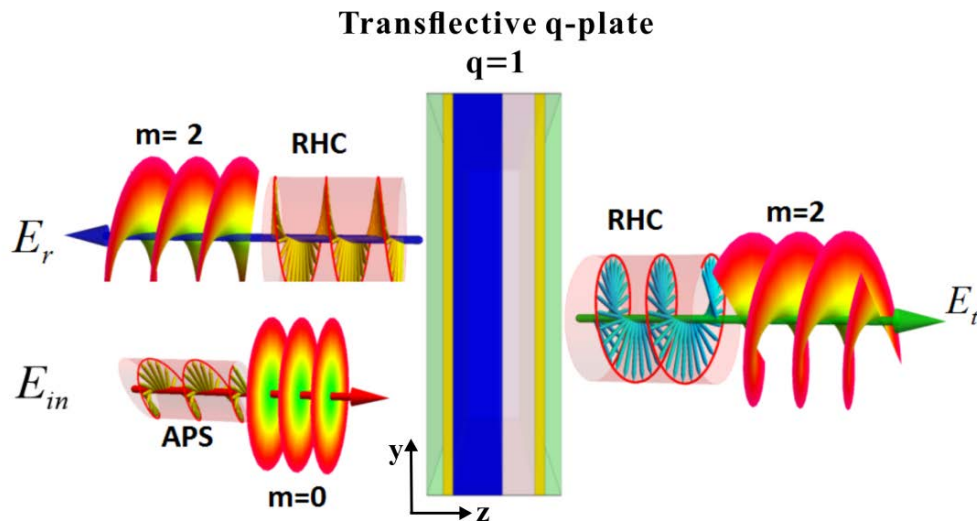


Fig. 2. Optical action pictorial illustration of a transfective type q-plate with  $q = 1$ ,  $\theta_0 = 0$  on an input planar light wave with arbitrary polarization state (APS). The transmissive and reflective light are RHC polarized and carry the helical modes with the topological charge  $m = 2$ .

### 3. Experiments and results

We point out that alignment technique is vital for the LC molecules to force arbitrary anchoring. The static LC cell alignment is determined by the boundary conditions and the elastic deformation energy of the LC molecules. In general, planar patterned LC devices can use the alignment methodologies of micro-nano rubbing, photo-alignment and Langmuir-Blodgett film. In addition, the anisotropic dispersive surface interaction forces of photo-polymerized layer can be used to align adjacent LC molecules [25,26].

On the basis of device fabrication and alignment methodologies, we assembled the polymerizable NLC and ChLC together for molecules arraying. The photo-alignment layers and polymer film surface were used to align them. Here, we spin-coated the photo-alignment material Dainippon Ink and Chemicals (SD1) 0.5% dissolved in demethylformamide (DMF) onto two cleaned glass substrates at 800 rpm for 5s and then 3000 rpm for 30s to form homogenous thin films and then heated on hotplates at 100°C for 5 minutes. These two substrates were exposed to the digital micro-mirror device (DMD) that impresses a topological charge 4 to the anchoring. Next, we prepared for 94 wt% of RM257 and 6 wt% of Irgacure184, and then they were diluted in toluene at 10:90 in weight. Then one of the substrates to spin-coat RM257 fulfilling half wave retardation of 633 nm, and this substrate should be cured with UV light for 2 minutes at a dosage of 2 J/cm<sup>2</sup> after each coating. After that, these two glasses were assembled together, and we used 18μm dielectric spacers to define the cell gap. Then, right-handed/left-handed ChLC mixtures composed of the NLC LC6200 ( $n_e = 1.753$  and  $n_o = 1.498$  at 20°C) doped with the chiral agent R811/S811 (22.7% in weight) were prepared. Lastly the cell was filled with a right-handed ChLC mixture. The fabrication process is illustrated schematically in Fig. 3(a), and the sketch of the device can be seen in Fig. 3(b). Figure 3(c) shows the image of q-plate between crossed linear polarizers.

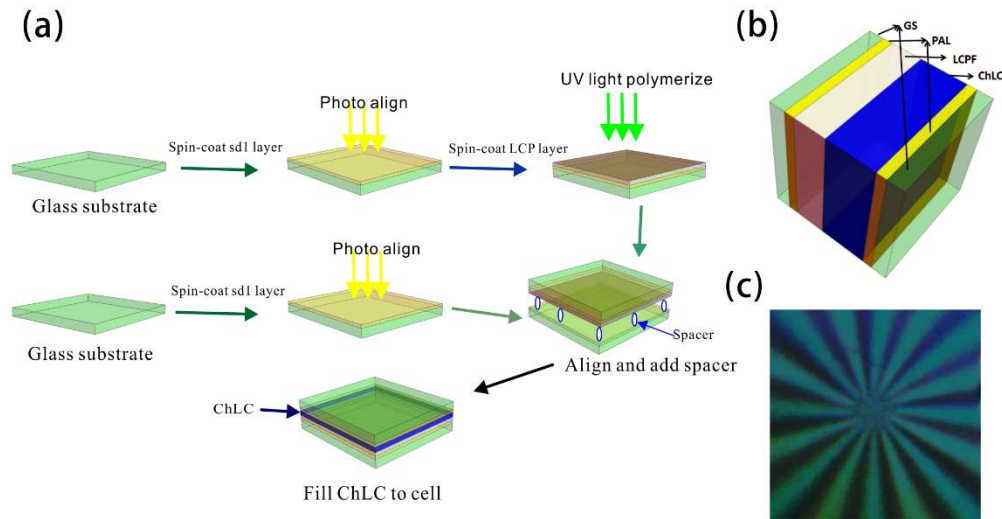


Fig. 3. (a) Schematic illustration of sample fabrication process. (b) sketch of the sample and material of each layer. LCPF, liquid crystal polymer film; PAL, photo-alignment layers; GS, glass substrates. (c) Photo of the transfective q-plate with  $q = 4$  under crossed linear polarizers.

We established an experimental setup to generate and photograph the transfective vortex beams as shown in Fig. 4(a). The operational characteristics of the fabricated q-plate were tested from the experimental setup in Fig. 4(a). A 633nm helium neon laser was used as source to illuminate the device. The beam splitter was used to view the reflected part. The transmitted and reflected patterns were collected by CMOS camera 1 and CMOS camera 2, which can be seen in Figs. 4(b)-4(d) and Figs. 4(f)-4(h) respectively. When a polarizer was inserted between laser and beam splitter, the linearly polarized (LP) incident light illuminated upon the transfective q-plate, and the transmitted and reflected optical patterns were represented in Figs. 4(b) and 4(f). In the case of adding a right-handed ChLC cell with uniform planar anchoring between polarizer and beam splitter, the RHC polarized light was reflected and LHC polarized light illuminated upon the transfective q-plate. The transmitted and reflected patterns were represented in Figs. 4(c) and 4(g). Figure 4(g) exhibited the weak reflected light that even cannot be seen clearly. Here, the transmissivity should be 100% and the reflectivity is 0% in theory. Similarly, when we removed the right-handed ChLC and replaced it with the left-handed ChLC cell, the LHC polarized light was reflected and RHC polarized light illuminated upon the transfective q-plate. The transmitted pattern and reflected pattern were represented in Figs. 4(d) and 4(h). Here, the transmissivity is 0% and the reflectivity is 100% in theory. Hence, Fig. 4(d) shows the transmitted light beam is vague. Here, it should be noted that the reflected beam and transmitted beam go through the same optical path length from q-plate to the corresponding camera. The theory and experiment indicate that the transmissivity and the reflectivity can be tuned arbitrarily by the incident light beam's polarization state. In addition, we measure the interference patterns of transmitted light and reflected light with the fundamental Gaussian light to ensure the topological charge of vortex beams, which can be seen in Figs. 4(e) and 4(i).

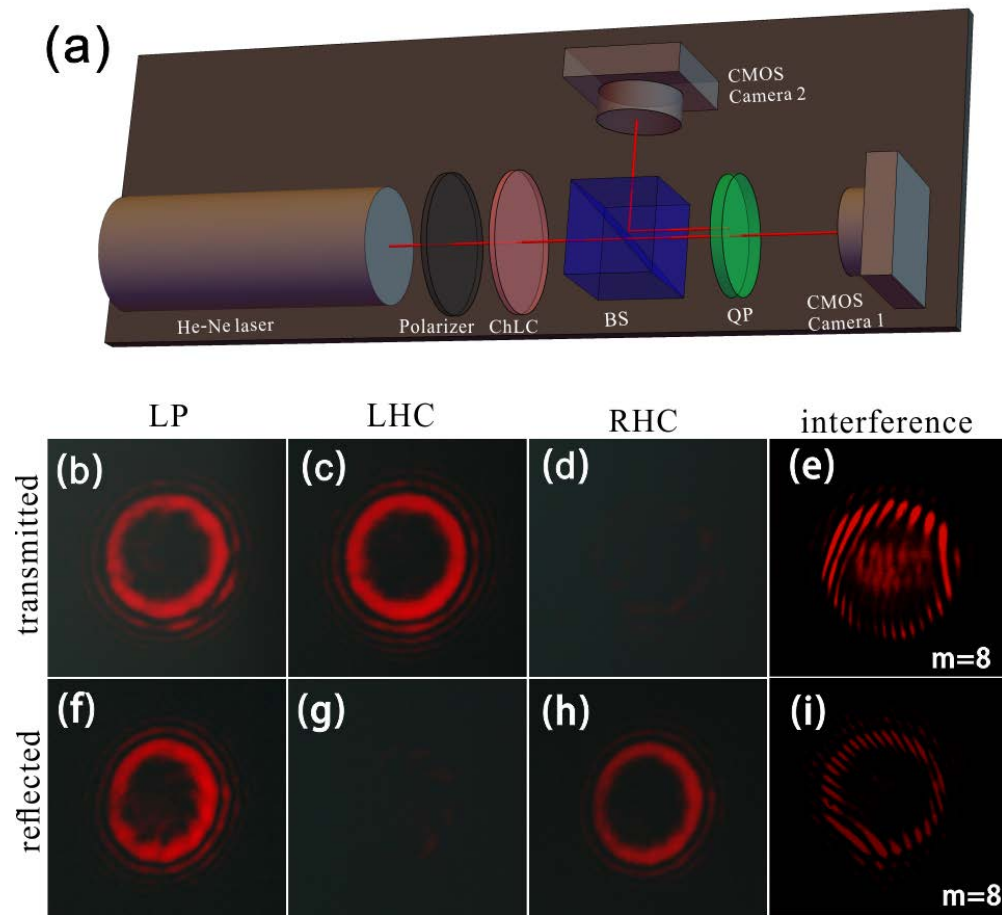


Fig. 4. (a) Experimental setup to generate transfllected vortices and measured intensity distribution by the interaction of Gaussian light with the transflreflective q-plate (QP). When linearly polarized (LP) light, LHC polarized light and RHC polarized light illuminate upon the QP in turn, transmitted optical intensity profiles were collected from CMOS Camera 1 which can be seen in (b) - (d). Reflected optical intensity profiles which were collected from CMOS Camera 2 can be seen in (f) - (h). (e) and (i) are the interference patterns of transmitted light and reflected light with the reference Gaussian light.

#### 4. Conclusions and discussions

In conclusion, we have proposed and experimentally demonstrated that the flat transflreflective element with the advantages of high efficiency, low cost, simple manufacturing process, and multi-functional integration represents many special features. It splits two orthogonal circularly polarized states and converts them into the same circularly polarized handedness. Moreover, the device has the integrated functions of generating the transmitted optical vortex and reflected optical vortex with 100% efficiency in theory. Furthermore, using the same fabrication methods, transflreflective elements with the complex phase distribution of light field can be fabricated by the technique of point-by-point photo-alignment [27,28]. On the one hand, the transflreflective elements possess the dual functions simultaneously without any additional transflreflector. On the other hand, transfllected optical vortices can be generated for any incident polarization state, besides, the amount of the transmitted and the reflected beams depend on the input polarization because of the selectivity of circular polarization. The transfllected optical vortices may play special roles in multi-dimensional optical display, sensing, imaging, communication and manipulation. Moreover, devices fabricated by

multilayer liquid crystalline materials based on the alignment technology have great potential in shaping arbitrary wavefronts, polarization and transfectivity.

## Funding

National Natural Science Foundation of China (NSFC) (61605046 and 11574079); Natural Science Foundation of Hunan Province (2018JJ3069); State Key Laboratory of Applied Optics; Fundamental Research Funds for the Central Universities of China.

## References

1. J. H. Poynting, "The wave motion of a revolving shaft, and a suggestion as to the angular momentum in a beam of circularly polarized light," *Proc. R. Soc. Lond., A Contain. Pap. Math. Phys. Character* **82**(557), 560–567 (1909).
2. L. Allen, M. W. Beijersbergen, R. J. C. Spreeuw, and J. P. Woerdman, "Orbital angular momentum of light and the transformation of Laguerre-Gaussian laser modes," *Phys. Rev. A* **45**(11), 8185–8189 (1992).
3. G. Molina Terriza, J. P. Torres, and L. Torner, "Twisted photons," *Nat. Phys.* **3**(5), 305–310 (2007).
4. L. Marrucci, C. Manzo, and D. Paparo, "Optical spin-to-orbital angular momentum conversion in inhomogeneous anisotropic media," *Phys. Rev. Lett.* **96**(16), 163905 (2006).
5. S. Slussarenko, A. Murauski, T. Du, V. Chigrinov, L. Marrucci, and E. Santamato, "Tunable liquid crystal q-plates with arbitrary topological charge," *Opt. Express* **19**(5), 4085–4090 (2011).
6. E. Karimi, B. Piccirillo, E. Nagali, L. Marrucci, and E. Santamato, "Efficient generation and sorting of orbital angular momentum eigenmodes of light by thermally tuned q-plates," *Appl. Phys. Lett.* **94**(23), 231124 (2009).
7. J. Kobashi, H. Yoshida, and M. Ozaki, "Planar optics with patterned chiral liquid crystals," *Nat. Photonics* **10**(6), 389–392 (2016).
8. R. Barboza, U. Bortolozzo, M. G. Clerc, and S. Residori, "Berry phase of light under Bragg reflection by chiral liquid crystal media," *Phys. Rev. Lett.* **117**(5), 053903 (2016).
9. M. Rafayelyan, G. Tkachenko, and E. Brasselet, "Reflective spin-orbit geometric phase from chiral anisotropic optical media," *Phys. Rev. Lett.* **116**(25), 253902 (2016).
10. J. Kobashi, H. Yoshida, and M. Ozaki, "Polychromatic optical vortex generation from patterned cholesteric liquid crystals," *Phys. Rev. Lett.* **116**(25), 253903 (2016).
11. M. Rafayelyan and E. Brasselet, "Bragg-Berry mirrors: reflective broadband q-plates," *Opt. Lett.* **41**(17), 3972–3975 (2016).
12. M. Rafayelyan, G. Agez, and E. Brasselet, "Ultra-broadband gradient-pitch Bragg-Berry mirrors," *Phys. Rev. A* **96**(4), 043862 (2017).
13. J. Kobashi, H. Yoshida, and M. Ozaki, "Broadband optical vortex generation from patterned cholesteric liquid crystals," *Mol. Cryst. Liq. Cryst.* **646**(1), 116–124 (2017).
14. M. Rafayelyan and E. Brasselet, "Spin-to-orbital angular momentum mapping of polychromatic light," *Phys. Rev. Lett.* **120**(21), 213903 (2018).
15. L. Marrucci, E. Karimi, S. Slussarenko, B. Piccirillo, E. Santamato, E. Nagali, and F. Sciarrino, "Spin-to-orbital conversion of the angular momentum of light and its classical and quantum applications," *J. Opt.* **13**(6), 064001 (2011).
16. M. J. Padgett and R. Bowman, "Tweezers with a twist," *Nat. Photonics* **5**(6), 343–348 (2011).
17. J. Wang, "Advances in communications using optical vortices," *Photon. Res.* **4**(5), B14–B28 (2016).
18. A. M. Yao and M. J. Padgett, "Orbital angular momentum: origins, behavior and applications," *Adv. Opt. Photonics* **3**(2), 161–204 (2011).
19. A. M. Tam, F. Fan, T. Du, W. Hu, W. L. Zhang, C. X. Zhao, X. Q. Wang, K. L. Ching, G. J. Li, H. L. Luo, V. Chigrinov, S. C. Wen, and H. S. Kwok, "Bifocal optical-vortex lens with sorting of the generated nonseparable spin-orbital angular-momentum states," *Phys. Rev. Appl.* **7**(3), 0304010 (2017).
20. P. Chen, B. Y. Wei, W. Ji, S. J. Ge, W. Hu, F. Xu, V. Chigrinov, and Y. Q. Lu, "Arbitrary and reconfigurable optical vortex generation: a high-efficiency technique using director-varying liquid crystal fork gratings," *Photon. Res.* **3**(4), 133–139 (2015).
21. W. Duan, P. Chen, S. J. Ge, B. Y. Wei, W. Hu, and Y. Q. Lu, "Helicity-dependent forked vortex lens based on photo-patterned liquid crystals," *Opt. Express* **25**(13), 14059–14064 (2017).
22. C. X. Zhao, F. Fan, T. Du, V. G. Chigrinov, and H. S. Kwok, "Multilayer photo-aligned thin-film structure for polarizing photonics," *Opt. Lett.* **40**(13), 2993–2996 (2015).
23. M. J. Tang, P. Chen, W. L. Zhang, A. M. Tam, V. G. Chigrinov, W. Hu, and Y. Q. Lu, "Integrated and reconfigurable optical paths based on stacking optical functional films," *Opt. Express* **24**(22), 25510–25514 (2016).
24. S. Slussarenko, A. Alberucci, C. P. Jisha, B. Piccirillo, E. Santamato, G. Assanto, and L. Marrucci, "Guiding light via geometric phases," *Nat. Photonics* **10**(9), 571–575 (2016).
25. M. Schadt, H. Seiberle, A. Schuster, and S. M. Kelly, "Photo-induced alignment and patterning of hybrid liquid crystalline polymer films on single substrates," *Jpn. J. Appl. Phys.* **34**(Part 2, No. 6B), L764–L767 (1995).
26. M. Schadt, K. Schmitt, V. Kozinkov, and V. Chigrinov, "Surface-induced parallel alignment of liquid crystals by linearly polymerized photopolymers," *Jpn. J. Appl. Phys.* **31**(1), 2155–2164 (1992).

27. H. Wu, W. Hu, H. C. Hu, X. W. Lin, G. Zhu, J. W. Choi, V. Chigrinov, and Y. Q. Lu, "Arbitrary photo-patterning in liquid crystal alignments using DMD based lithography systems," *Opt. Express* **20**(15), 16684–16689 (2012).
28. J. Kim, Y. Li, M. N. Miskiewicz, C. Oh, M. W. Kudenov, and M. J. Escuti, "Fabrication of ideal geometric-phase holograms with arbitrary wavefronts," *Optica* **2**(11), 958–964 (2015).